

Learning Autonomous Ultrasound via Latent Task Representation and Robotic Skills Adaptation

Xutian Deng*, Junnan Jiang[†], Wen Cheng[‡] and Miao Li[§]

*School of Computer Science, Wuhan University, Wuhan 430072, China

Email: dengxutian@whu.edu.cn

[†]School of Power and Mechanical Engineering, Wuhan University, Wuhan 430072, China

[‡]Hospital of Wuhan University, Wuhan University, Wuhan 430072, China

[§]School of Microelectronics, Wuhan University, Wuhan 430072, China

Email: miao.li@whu.edu.cn

Abstract—As medical ultrasound is becoming a prevailing examination approach nowadays, robotic ultrasound systems can facilitate the scanning process and prevent professional sonographers from repetitive and tedious work. Despite the recent progress, it is still a challenge to enable robots to autonomously accomplish the ultrasound examination, which is largely due to the lack of a proper task representation method, and also an adaptation approach to generalize learned skills across different patients. To solve these problems, we propose the latent task representation and the robotic skills adaptation for autonomous ultrasound in this paper. During the offline stage, the multimodal ultrasound skills are merged and encapsulated into a low-dimensional probability model through a fully self-supervised framework, which takes clinically demonstrated ultrasound images, probe orientations, and contact forces into account. During the online stage, the probability model will select and evaluate the optimal prediction. For unstable singularities, the adaptive optimizer fine-tunes them to near and stable predictions in high-confidence regions. Experimental results show that the proposed approach can generate complex ultrasound strategies for diverse populations and achieve significantly better quantitative results than our previous method.

I. INTRODUCTION

Medical ultrasound has been widely employed in routine clinical examinations, which faces two main challenges: 1) long-term training for professional skills [1] and 2) physical injury caused by repetitive work [14]. To this end, robotic ultrasound systems have been proposed to overcome these challenges [19, 9], which can be further divided into teleoperated and autonomous [11, 16, 20] ones. Autonomous ultrasound contains three major spectra, human-guided [21], vision-based [7, 8] and policy-based, according to the complexity of strategies. Policy-based systems highlight the learning approaches of general ultrasound skills, e.g. learning from demonstrations [5, 3, 18] and reinforcement learning [15, 10, 17]. However, these studies have some weaknesses: 1) Since autonomous ultrasound is a high-dimensional robotic task, some indispensable modalities in latent task representation are ignored, e.g. probe orientations and contact forces. 2) The generalization of learned skills, i.e. the adaptation to patients with different physical conditions, has not been proposed and emphasized.

Following these studies, our work improves the involved modalities with a fully self-supervised framework to per-

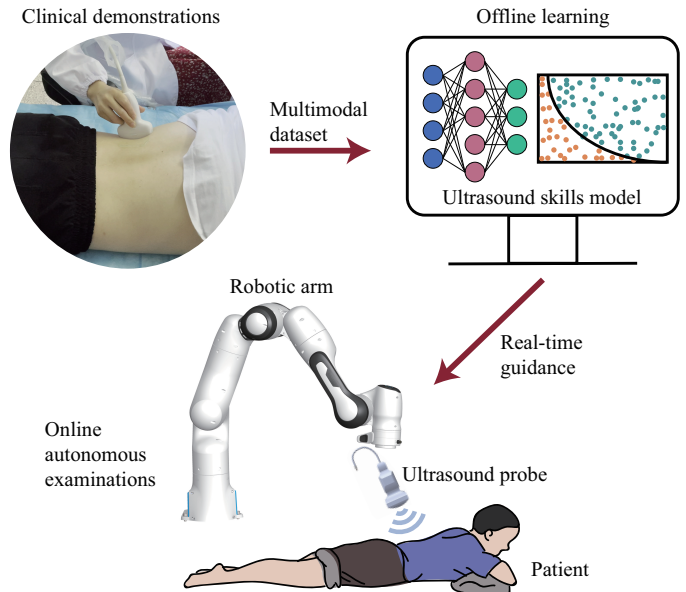


Fig. 1: The workflow of autonomous ultrasound. First, sonographers' clinical demonstrations for diverse patients are collected. Then, these demonstrated experiences are encapsulated into an ultrasound skills model at the offline stage. Finally, at the online stage, the robotic ultrasound system performs an autonomous examination for a non-previous patient through learned skills.

form multimodal fusion and task representation. Besides, we propose and verify an adaptive ultrasound strategy, which abstracts the learned skills into a probability model and accordingly fine-tunes predictions. Fig. 1 shows the workflow of autonomous ultrasound. Our main contribution is twofold:

- For modeling ultrasound skills, a fully self-supervised latent representation method is proposed, which takes clinically demonstrated ultrasound images, probe orientations, and contact forces into account.
- For improving the adaptation of learned skills, we propose a probability-based method to evaluate and fine-tune the ultrasound probe's orientations and contact forces, which enhances the algorithm's robustness and generalization for patients with different physical conditions.

II. METHODOLOGY

Fig. 2 presents the framework of methodology in this paper. Our goal is to learn freehand ultrasound skills from profes-

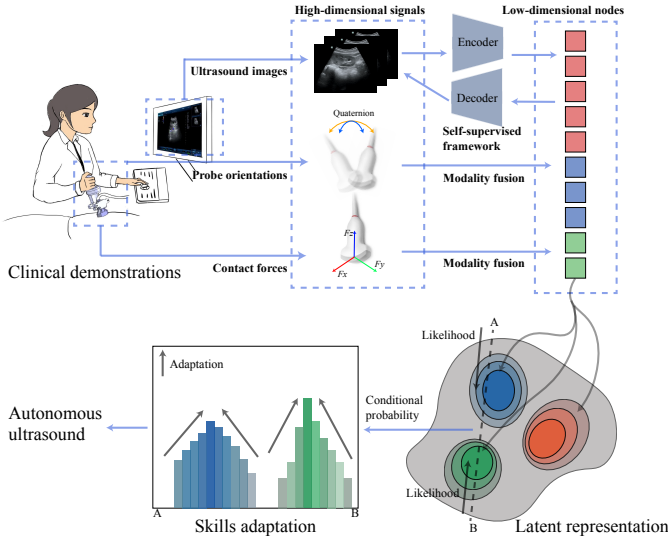


Fig. 2: The framework of latent task representation and robotic skills adaptation. Synchronous sequences are demonstrated and embedded into latent space as discrete nodes. The global distribution is learned by a probability model. The latent state’s likelihood can be regarded as an evaluation. Any low-likelihood nodes will be judged as unstable, and an adaptive optimizer will fine-tune them to near and stable predictions in high-confidence regions.

sional sonographers’ demonstrations and further generalize them to some kind of adaptive robotic ultrasound skills for patients of different ages, genders, and body physiques.

A. Problem Formulation

The data involved in the training process is as follows:

- $D = \{d_1, d_2, \dots, d_N\} = \{(x_i, p_i, f_i)\}_{i=1 \dots N}$ denotes a high-dimensional dataset with N observations.
- $x_i \in \mathbb{R}^{224 \times 224 \times 1}$ denotes the i -th collected ultrasound image with cropped size.
- $p_i \in \mathbb{R}^4$ denotes the probe orientation (quaternion).
- $f_i \in \mathbb{R}^6$ denotes the contact force/torque.

Additionally, $w_i = \{p_i, f_i\}$ is the variable directly related to robot control. To perform autonomous ultrasound based on a prior dataset D , the target function is described as:

$$\begin{aligned} \max \mathbb{E}[\log P(x_t, \hat{w}_{t+1} | D)] \\ \text{s.t. } \hat{w}_{t+1} = f_{AU}(x_t, w_t | D), \end{aligned} \quad (1)$$

where \hat{w}_{t+1} is the prediction, $f_{AU}(\cdot)$ denotes the robotic policy, and $P(\cdot)$ represents the conditional probability.

B. Latent Representation and Skills Adaptation

To latently represent the autonomous ultrasound task, we employ self-supervised learning to determine the mapping rule from high- to low-dimensional spaces, and v_i denotes the feature vector of x_i . The represented demonstrations are equivalent to $D' = \{(v_i, p_i, f_i)\}_{i=1 \dots N}$. To this end, demonstrations are replaced by nodes (concatenations of v , p , and f) in latent space, and learning ultrasound skills is equal to finding a proper distribution to measure the conditional probability in Eq. 1. We assume nodes in latent space follow the Gaussian

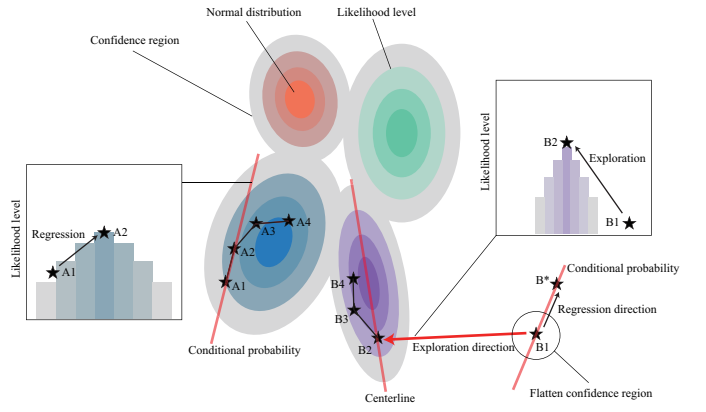


Fig. 3: The adaptation scheme of learned ultrasound skills in this paper. If an embedded state is mapped to a high-likelihood node, such as $A1$, then the state will be judged as stable. In this case, the optimization is a step-by-step iterative process. In another case, the embedded state is in a low-likelihood region and judged as unstable, such as $B1$. For this node, the local likelihood does not change that much and the confidence tends to be small and flat. The singularity will be straightly fixed to the nearest Gaussian distribution (from $B1$ to $B2$) and avoid following the gradient of conditional probability, which usually produces a relatively random result (from $B1$ to B^*).

mixture distribution:

$$P(D' | \Omega) = \sum_{k=1}^K \pi_k \mathcal{N}(D' | \mu_k, \Sigma_k). \quad (2)$$

where π_k is the prior of k -th Gaussian component, $\mathcal{N}(\mu_k, \Sigma_k)$ is the Gaussian distribution with mean μ_k and covariance Σ_k .

1) *Prediction Step*: The learned ultrasound skills can be reproduced by Gaussian Mixture Regression (GMR) [2], and the conditional expectation of w given v is defined as:

$$\begin{aligned} P(w|v) \sim \mathcal{N}(\hat{\mu}^w, \hat{\Sigma}^{w,w}), \\ \hat{\mu}^w = \sum_{k=1}^K \pi_k \hat{\mu}_k^w, \quad \hat{\Sigma}^{w,w} = \sum_{k=1}^K \pi_k^2 \hat{\Sigma}_k^{w,w}. \end{aligned} \quad (3)$$

2) *Evaluation Step*: The likelihood range $[a_k^{m\sigma}, b_k^{m\sigma}]$ of k -th Gaussian component at m standard deviation is:

$$\begin{aligned} a_k^{m\sigma} = \min Lik_k^{m\sigma}(d), \\ b_k^{m\sigma} = \max Lik_k^{m\sigma}(d). \end{aligned} \quad (4)$$

The stability of $\hat{d} = \{v, \hat{w}\}$ can be measured by:

$$\begin{aligned} \text{Case1: } Lik_k(\hat{d}) \in [a_k^{m\sigma}, b_k^{m\sigma}], \exists k \in [1, 2, \dots, K] \\ \text{Case2: } Lik_k(\hat{d}) \notin [a_k^{m\sigma}, b_k^{m\sigma}], \forall k \in [1, 2, \dots, K] \end{aligned} \quad (5)$$

If the prediction’s likelihood is subject to *Case1*, it will be considered stable. Else if its likelihood is subject to *Case2*, the prediction will be considered unstable and needs to be fine-tuned in the following adaptation stage.

3) *Adaptation Step*: The adaptation scheme is shown in Fig. 3. For unstable cases, selecting the GMR result in Eq. 3 as the local optimum may be invalid. That is because similar samples are scarce in demonstrations, and the probability model is non-referential to singularities. To avoid this, \hat{w} will be adjusted through the local exploration [13]:

$$\hat{w} = \arg \min_{\mu_k^w} l_k \quad \text{s.t. } k = 1, 2, \dots, K, \quad (6)$$

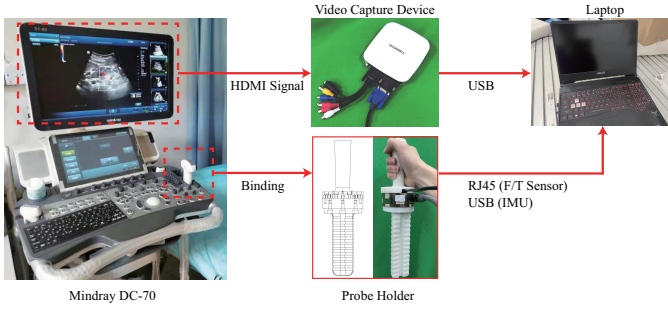


Fig. 4: The hardware system for clinical experiments.

where l_k is the Mahalanobis distance between the prediction and the center of k -th Gaussian component.

III. EXPERIMENTS

A. Clinical Demonstrations

This work was supported and supervised by the Medical Ethics Committee, School of Medicine, Wuhan University, Ethics Statement No.WHU2021-PMC002. Our experimental setup is shown in Fig. 4. The clinical experiment was at the Hospital of Wuhan University. The sonographer performed 5 times of left kidney examinations for each volunteer. The recording frequency was 10 Hz. A whole demonstration was started with the sonographer vertically holding the probe holder upon the target part. After 3 ~ 5 seconds from the coordinate alignment and gravity calibration, the sonographer would start to perform freehand ultrasound examinations. Each demonstration lasted 40 ~ 80 seconds. A total of 24 volunteers (14 males and 10 females) participated in this experiment. In order to make the individual differences in demonstrations more typical, we not only considered gender but also deliberately included people of different degrees of obesity and age groups in the experiment. Volunteers' BMI ranged from 16.4 (underweight) to 26.7 (overweight), and their ages ranged from 19 to 67. Totally, there were 53571 sets of multimodal data in our dataset.

B. Latent Representation

The ultrasound skills model first learns to encode ultrasound images into feature vectors and then concatenates three modalities as low-dimensional nodes. Then, the embedded nodes in latent space are encapsulated into a Gaussian Mixture Model (GMM). The modalities fusion pipeline is presented in Fig. 5. In detail, the ultrasound images' feature extraction is performed by Masked Auto Encoder (MAE) [6]. The raw ultrasound images are with a 1920×1080 resolution. Through cropping, scaling, and grayscale, they are converted to $1 \times 224 \times 224$ preprocessed images. Each preprocessed one is divided into 8×8 patches with the size of 28×28 . A random selector picks 40 out of 64 patches and the rest are masked out. The remaining 40 patches are reshaped to a $1 \times 40 \times 784$ feature vector, and thus processed by the encoder and decoder modules.

The $1 \times 40 \times 784$ feature vector is too large to merge with the other modalities. Therefore, a channel summation is added to

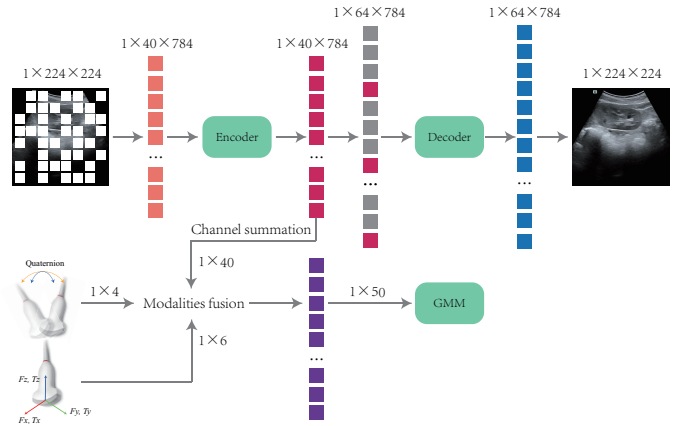


Fig. 5: The modalities fusion framework. The encoder-decoder backbone is performed by Masked Autoencoder [6], and fusion is performed by channel summation and concatenating.

compress 784 values in each channel into one single feature value, and the ultrasound modality is replaced by a 1×40 feature vector. Now, by concatenating the 1×40 feature vector, 1×4 quaternion vector, and 1×6 force/torque vector, every state in original demonstrations can be mapped to a node in 50D latent space. To model these low-dimensional nodes as a probability distribution, we use the GMM with 16 Gaussian components (about 40000 parameters).

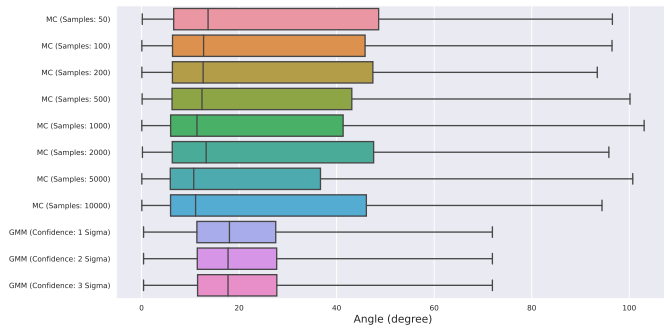
C. Skills Adaptation

Once parameters of MAE and GMM are learned, the probability model in Eq. 1 is equally determined. In this way, autonomous ultrasound can be reproduced by GMR. However, singularities are inevitable since demonstrations are always insufficient to fully cover all cases. To this end, we propose the robotic skills adaptation to alleviate this problem, which computes the likelihood bounds for every Gaussian distribution in m standard deviation, and fine-tunes those unstable nodes with low likelihoods.

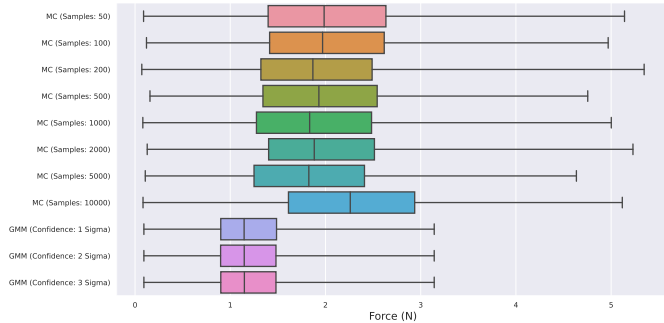
Our baseline is the Monte Carlo (MC) method [4, 12], where the probability model is replaced by a Multilayer Perceptron (MLP) model. Experimental results have shown that the MC method could learn demonstrated ultrasound skills and reproduce an expert-like strategy. But it tends to

TABLE I: Summary results of MC and GMM methods in five tasks.

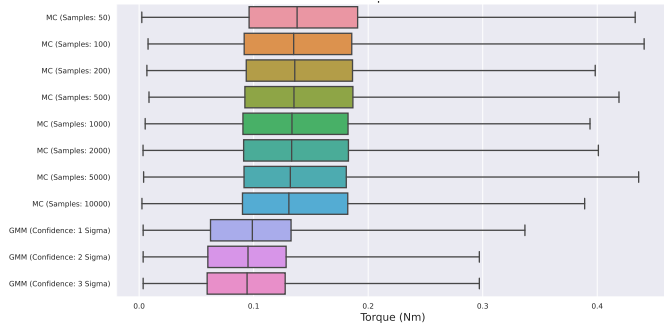
Methods	Pose error (degree)	Force error (N)	Torque error (Nm)	FPS	
MC	50 samples	27.36 ± 26.08	2.05 ± 0.86	0.14 ± 0.06	66.07
	100 samples	26.43 ± 25.90	2.04 ± 0.85	0.14 ± 0.06	43.75
	200 samples	26.65 ± 26.07	1.94 ± 0.83	0.14 ± 0.06	34.97
	500 samples	25.55 ± 25.43	1.98 ± 0.85	0.14 ± 0.06	15.00
	1000 samples	24.69 ± 25.32	1.92 ± 0.85	0.14 ± 0.06	7.40
	2000 samples	27.06 ± 26.26	2.01 ± 0.87	0.13 ± 0.06	3.64
	5000 samples	23.63 ± 25.17	1.87 ± 0.83	0.13 ± 0.06	1.36
	10000 samples	25.24 ± 25.79	2.29 ± 0.91	0.13 ± 0.06	0.61
GMM (Ours)	1-sigma region	20.63 ± 12.29	1.22 ± 0.47	0.10 ± 0.05	304.98
	2-sigma region	20.64 ± 12.17	1.21 ± 0.45	0.09 ± 0.05	312.01
	3-sigma region	20.61 ± 12.11	1.21 ± 0.46	0.09 ± 0.04	306.22



(a) Pose error



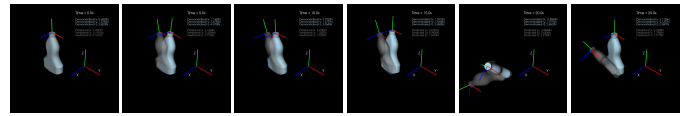
(b) Force error



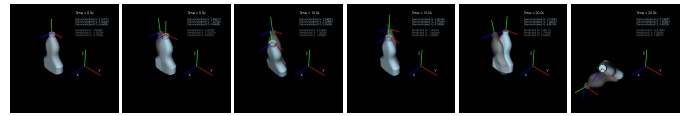
(c) Torque error

Fig. 6: Boxplots of MC and GMM methods in five tasks.

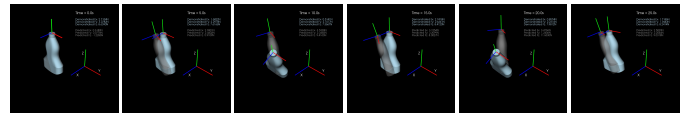
sacrifice more computing resources to acquire more acceptable results. Therefore, we study the upper limitation of the MC method and make a quantitative comparison with the GMM method in this experiment. In detail, 1σ , 2σ , and 3σ confidence regions are chosen for the GMM method respectively. While the numbers of samples are 50, 100, 200, 500, 1000, 2000, 5000, and 10000 in the MC method. For the intra-patient experiment, the first 4 demonstrations of every volunteer are used for training and the last for evaluation. For the inter-patient experiment, all demonstrations of 1 ~ 22 volunteers are used for training, and those of 23 ~ 24 volunteers are used for evaluation. In addition, we further evaluate the proposed method in different tasks (inter-gender, inter-age, and inter-BMI tasks) with significantly larger individual differences to explore our method's robustness and generalization. Summary results are presented in Fig. 6 and TABLE. I. The 3σ GMM policy (gray) is visualized in Fig. 7, which shows great agreement with the sonographer's demonstrations (blue).



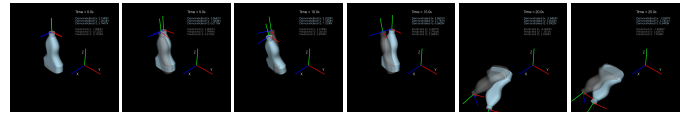
(a) No.1 volunteer, male, age 19, BMI 17.99 (underweight).



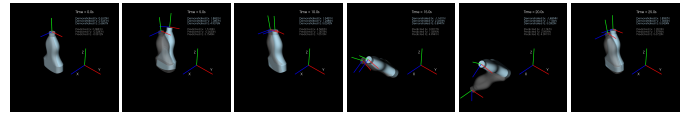
(b) No.5 volunteer, male, age 23, BMI 26.58 (overweight).



(c) No.12 volunteer, male, age 36, BMI 19.13 (normal).



(d) No.13 volunteer, female, age 67, BMI 25.39 (overweight).



(e) No.15 volunteer, female, age 22, BMI 22.86 (normal).

Fig. 7: Visualization of autonomous ultrasound tasks.

IV. CONCLUSION

Learning autonomous strategies for robotic ultrasound systems is still unsolved, which is mainly related to the absence of two fundamental capabilities: a proper representation method to model and reproduce, and an adaptive method to generalize and adjust the learned ultrasound skills. In this paper, we propose to learn robotic ultrasound skills from clinical freehand examinations demonstrated by a professional sonographer with latent representation and skills adaptation, which highlights feasibility and generalization for patients with different physical conditions. During the offline stage, the multimodal ultrasound skills are encapsulated into a low-dimensional probability model through a fully self-supervised framework, which takes ultrasound images, probe orientations, and contact forces into account. During the online stage, the optimal prediction will be selected and evaluated by the probability model. For any singularities with unstable and uncertain states, the adaptive optimizer fine-tunes them to near and stable predictions in high-confidence regions. The experimental results in intra-patient, inter-patient, inter-gender, inter-age, and inter-BMI tasks show that the proposed approach can generate complex strategies for diverse populations, with accuracy and speed significantly better than our previous method.

ACKNOWLEDGMENTS

This work was supported by the Fundamental Research Funds for the Central Universities (No.2042023KF0110).

REFERENCES

- [1] Peter H Arger, Susan M Schultz, Chandra M Sehgal, Theodore W Cary, and Judith Aronchick. Teaching medical students diagnostic sonography. *Journal of Ultrasound in Medicine*, 24(10):1365–1369, 2005.
- [2] Aude Billard, Sylvain Calinon, Ruediger Dillmann, and Stefan Schaal. Robot programming by demonstration. In *Springer Handbook of Robotics*, pages 1371–1394. Springer Berlin Heidelberg, 2008.
- [3] Xutian Deng, Yiting Chen, Fei Chen, and Miao Li. Learning robotic ultrasound scanning skills via human demonstrations and guided explorations. In *2021 IEEE International Conference on Robotics and Biomimetics (ROBIO)*, pages 372–378, 2021.
- [4] Xutian Deng, Ziwei Lei, Yi Wang, Wen Cheng, Zhao Guo, Chenguang Yang, and Miao Li. Learning ultrasound scanning skills from human demonstrations. *SCIENCE CHINA Information Sciences*, 65(8):184201, 2022.
- [5] Richard Droste, Lior Drukker, Aris T Papageorghiou, and J Alison Noble. Automatic probe movement guidance for freehand obstetric ultrasound. In *International Conference on Medical Image Computing and Computer-Assisted Intervention*, pages 583–592, 2020.
- [6] Kaiming He, Xinlei Chen, Saining Xie, Yanghao Li, Piotr Dollár, and Ross Girshick. Masked autoencoders are scalable vision learners. In *Proceedings of the IEEE/CVF Conference on Computer Vision and Pattern Recognition (CVPR)*, pages 16000–16009, 2022.
- [7] Zhongliang Jiang, Matthias Grimm, Mingchuan Zhou, Javier Esteban, Walter Simson, Guillaume Zahnd, and Nassir Navab. Automatic normal positioning of robotic ultrasound probe based only on confidence map optimization and force measurement. *IEEE Robotics and Automation Letters*, 5(2):1342–1349, 2020.
- [8] Zhongliang Jiang, Felix Duellmer, and Nassir Navab. Dopus-net: Quality-aware robotic ultrasound imaging based on doppler signal. *IEEE Transactions on Automation Science and Engineering*, 2023.
- [9] Zhongliang Jiang, Septimiu E Salcudean, and Nassir Navab. Robotic ultrasound imaging: State-of-the-art and future perspectives. *Medical Image Analysis*, page 102878, 2023.
- [10] Keyu Li, Jian Wang, Yangxin Xu, Hao Qin, Dongsheng Liu, Li Liu, and Max Q.-H. Meng. Autonomous navigation of an ultrasound probe towards standard scan planes with deep reinforcement learning. In *2021 IEEE International Conference on Robotics and Automation (ICRA)*, pages 8302–8308, 2021.
- [11] Keyu Li, Yangxin Xu, and Max Q.-H. Meng. An overview of systems and techniques for autonomous robotic ultrasound acquisitions. *IEEE Transactions on Medical Robotics and Bionics*, 3(2):510–524, 2021.
- [12] Miao Li and Xutian Deng. Learning Robotic Ultrasound Skills from Human Demonstrations. In *Cognitive Robotics*. IntechOpen, 2022.
- [13] Miao Li, Yasemin Bekiroglu, Danica Kragic, and Aude Billard. Learning of grasp adaptation through experience and tactile sensing. In *2014 IEEE/RSJ International Conference on Intelligent Robots and Systems*, pages 3339–3346. Ieee, 2014.
- [14] Carmel Murphy and Andre Russo. An update on ergonomic issues in sonography. *Healthcare Benefit Trust*, 2000.
- [15] Guochen Ning, Xinran Zhang, and Hongen Liao. Autonomous robotic ultrasound imaging system based on reinforcement learning. *IEEE Transactions on Biomedical Engineering*, 68(9):2787–2797, 2021.
- [16] Guochen Ning, Hanying Liang, Xinran Zhang, and Hongen Liao. Autonomous Robotic Ultrasound Vascular Imaging System With Decoupled Control Strategy for External-Vision-Free Environments. *IEEE Transactions on Biomedical Engineering*, 2023.
- [17] Guochen Ning, Hanying Liang, Xinran Zhang, and Hongen Liao. Inverse-reinforcement-learning-based robotic ultrasound active compliance control in uncertain environments. *IEEE Transactions on Industrial Electronics*, 2023.
- [18] Deepak Raina, SH Chandrashekhara, Richard Voyles, Juan Wachs, and Subir Kumar Saha. Robotic Sonographer: Autonomous Robotic Ultrasound using Domain Expertise in Bayesian Optimization. In *2023 IEEE International Conference on Robotics and Automation (ICRA)*, pages 6909–6915. IEEE, 2023.
- [19] Septimiu E. Salcudean, Hamid Moradi, David G. Black, and Nassir Navab. Robot-assisted medical imaging: a review. *Proceedings of the IEEE*, 110(7):951–967, 2022.
- [20] Junchen Wang, Chunheng Lu, Yifei Lv, Siqin Yang, Mingbo Zhang, and Yu Shen. Task Space Compliant Control and Six-Dimensional Force Regulation Toward Automated Robotic Ultrasound Imaging. *IEEE Transactions on Automation Science and Engineering*, 2023.
- [21] Ziwen Wang, Baoliang Zhao, Peng Zhang, Liang Yao, Qiong Wang, Bing Li, Max Q.-H. Meng, and Ying Hu. Full-coverage path planning and stable interaction control for automated robotic breast ultrasound scanning. *IEEE Transactions on Industrial Electronics*, 70(7):7051–7061, 2023.

Supplementary Materials: Learning Autonomous Ultrasound via Latent Task Representation and Robotic Skills Adaptation

Xutian Deng*, Junnan Jiang[†], Wen Cheng[‡] and Miao Li[§]

*School of Computer Science, Wuhan University, Wuhan 430072, China
Email: dengxutian@whu.edu.cn

[†]School of Power and Mechanical Engineering, Wuhan University, Wuhan 430072, China

[‡]Hospital of Wuhan University, Wuhan University, Wuhan 430072, China

[§]School of Microelectronics, Wuhan University, Wuhan 430072, China
Email: miao.li@whu.edu.cn

SUPPLEMENTARY #1: PHYSICAL INFORMATION OF VOLUNTEERS

TABLE I: Physical condition of 24 clinical volunteers.

Volunteer	Age	Gender	Height (m)	Weight (kg)	BMI	Assessment
1	19	Male	1.65	49	17.9982	Underweight
2	35	Male	1.74	68	22.4600	Normal
3	27	Male	1.72	79	26.7036	Overweight
4	25	Male	1.72	62	20.9573	Normal
5	23	Male	1.84	90	26.5832	Overweight
6	24	Male	1.62	46	17.5278	Underweight
7	23	Male	1.79	81	25.2801	Overweight
8	23	Male	1.76	53	17.1100	Underweight
9	22	Male	1.77	80	25.5354	Overweight
10	24	Male	1.82	72	21.7365	Normal
11	27	Male	1.81	68	20.7564	Normal
12	36	Male	1.68	54	19.1327	Normal
13	67	Female	1.60	65	25.3906	Overweight
14	24	Male	1.70	67	23.1834	Normal
15	22	Female	1.62	60	22.8624	Normal
16	23	Male	1.70	55	19.0311	Normal
17	19	Female	1.58	46	18.4265	Underweight
18	24	Female	1.63	51	19.1953	Normal
19	25	Female	1.55	55	22.8928	Normal
20	21	Female	1.69	60	21.0077	Normal
21	19	Female	1.54	39	16.4446	Underweight
22	19	Female	1.61	55	21.2183	Normal
23	24	Female	1.58	50	20.0288	Normal
24	25	Female	1.62	49	18.6709	Normal

SUPPLEMENTARY #2: HARDWARE DETAILS

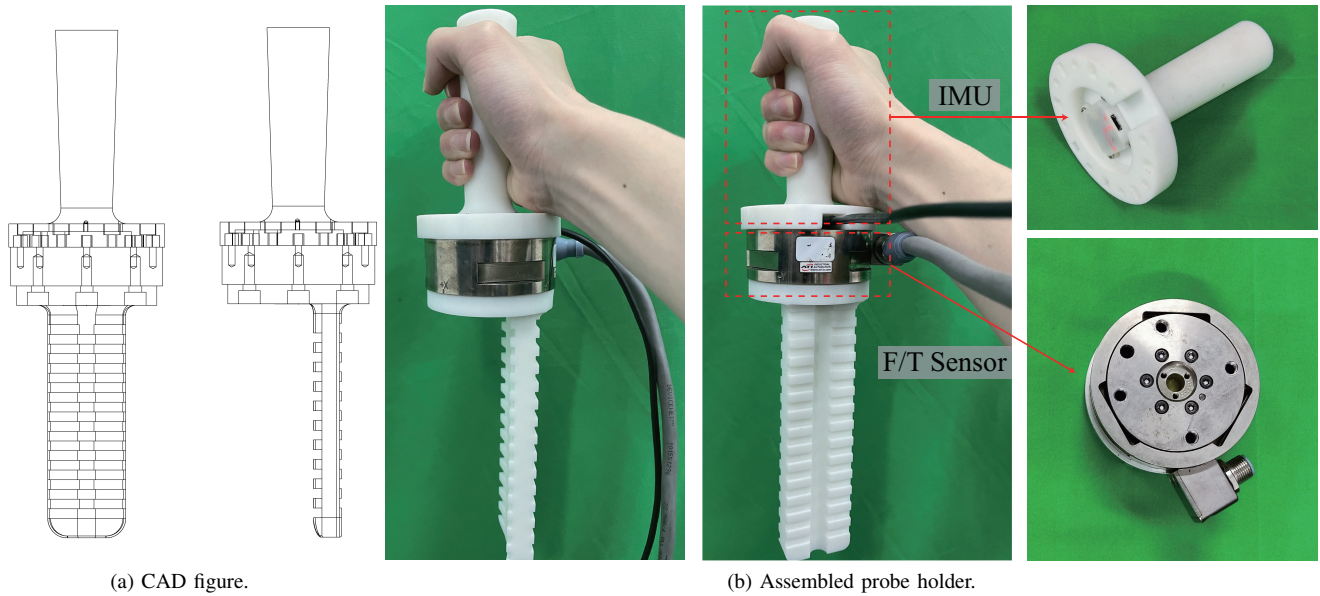
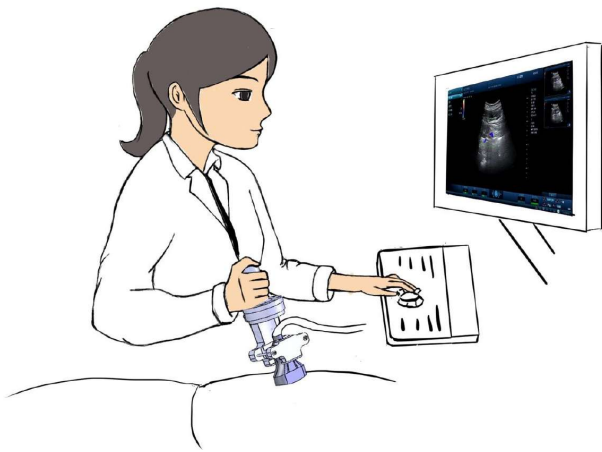


Fig. 1: Some details about the probe holder in our experiment. This probe holder has two main sensors to monitor the real-time ultrasound demonstrations: a build-in IMU (ICM20948 module and up to 200 Hz) and a 6D force/torque sensor (ATI Gamma F/T sensor whose resolutions are 1/80 N, 1/80 N, and 1/40 N in three orthogonal directions). During the clinical experiment, the ultrasound probe will be mounted at the bottom, and the sonographer can hold the top handle to perform ultrasound examinations.

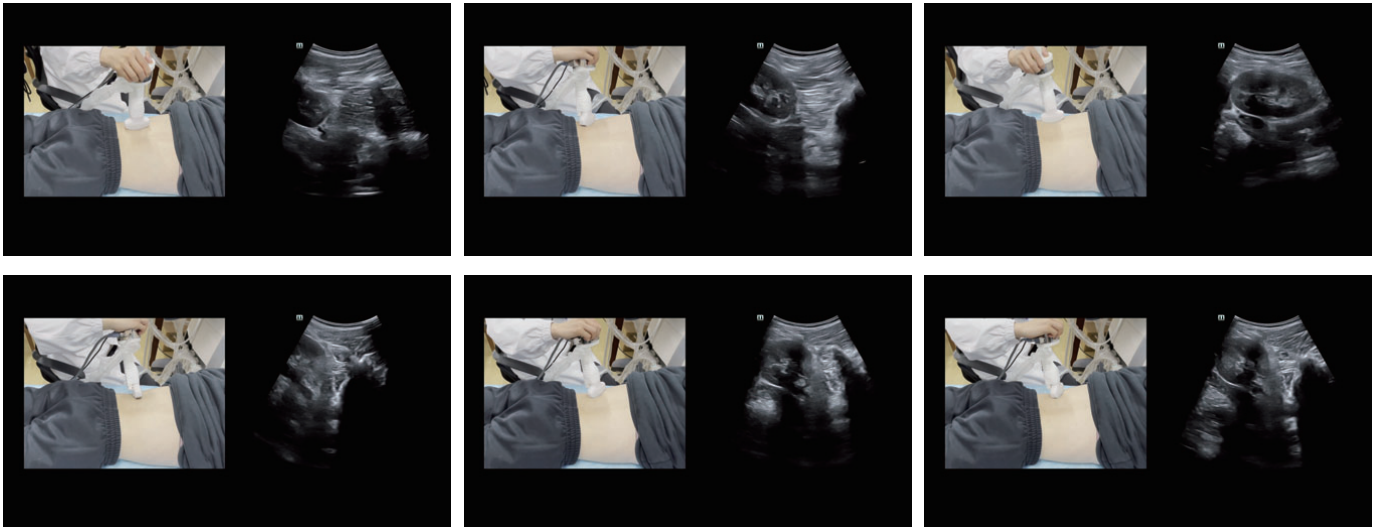
SUPPLEMENTARY #3: EXPERIMENTAL SNAPSHOTS



(a) Stick figure.



(b) Clinical snapshot.



(c) Freehand ultrasound tricks and the corresponding ultrasound images.

Fig. 2: Some snapshots in clinical demonstration experiments. The instruction for hardware usage is shown in (a), by which the ultrasound videos, probe orientations, and contact forces were collected. An experimental snapshot is presented in (b). Some freehand ultrasound tricks of the sonographer and the corresponding ultrasound images are shown in (c). The whole demonstration started with the sonographer vertically holding the probe holder upon the target region. After 3 ~ 5 seconds from the coordinate alignment and gravity calibration, the sonographer started to perform freehand ultrasound examinations. Each demonstration lasted 40 ~ 80 seconds.

SUPPLEMENTARY #4: VISUALIZED GMM

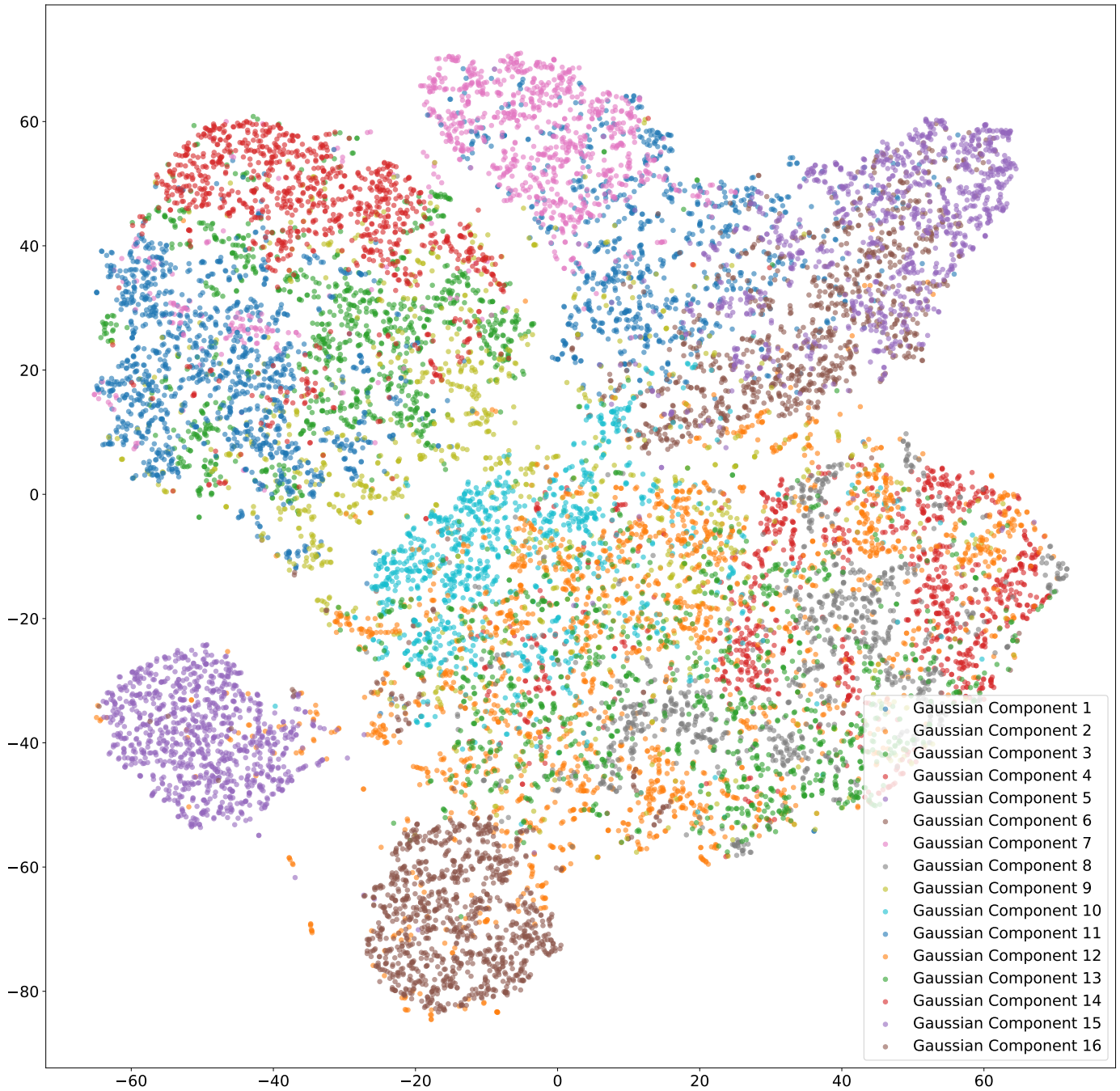
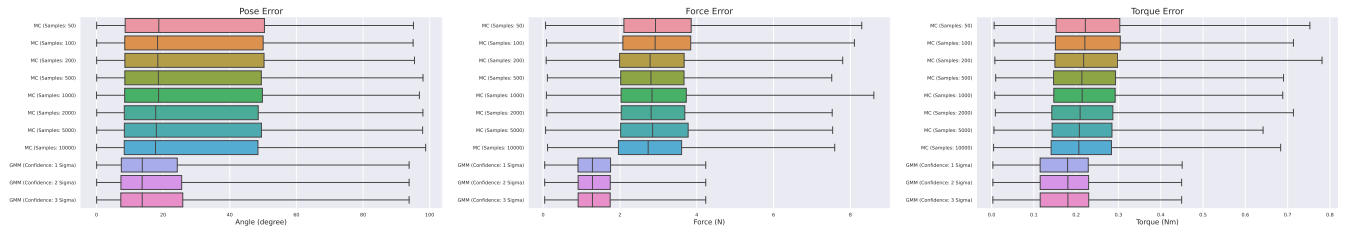
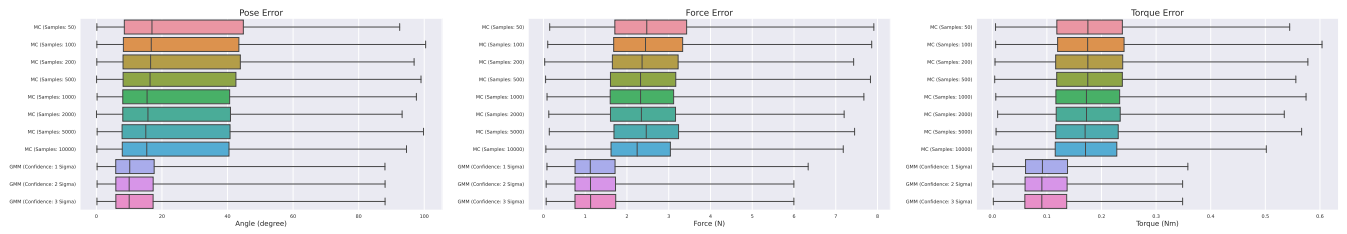


Fig. 3: Gaussian distributions visualized by the t-SNE algorithm in the 2D plane.

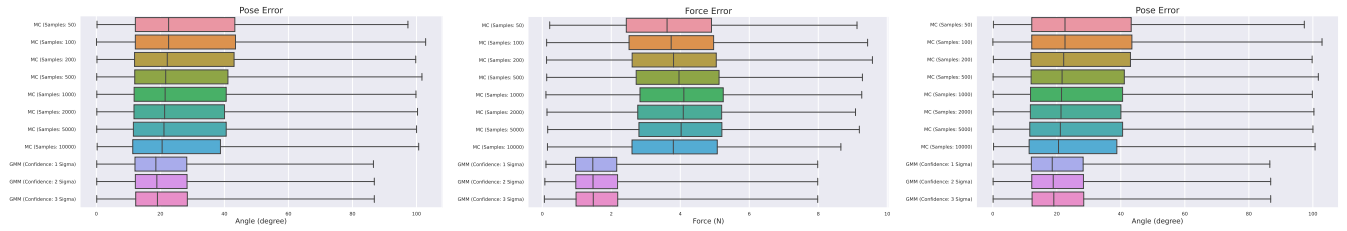
SUPPLEMENTARY #5: EXPERIMENTAL RESULTS OF INTER-GENDER, INTER-AGE, AND INTER-BMI TASKS



(a) Experimental result of the inter-gender task



(b) Experimental result of the inter-age task



(c) Experimental result of the inter-BMI task

Fig. 4: Experimental results of inter-gender, inter-age, inter-BMI tasks.

TABLE II: Experimental result of the inter-gender task.

Methods	Pose error (degree)	Force error (N)	Torque error (Nm)	FPS	
MC methods	50 samples	29.3762 ± 24.6150	3.0254 ± 1.2453	0.2336 ± 0.1082	66.8829
	100 samples	29.0951 ± 24.6043	3.0084 ± 1.2499	0.2334 ± 0.1089	42.6738
	200 samples	29.0945 ± 24.5366	2.8858 ± 1.2104	0.2301 ± 0.1075	34.4192
	500 samples	29.0272 ± 24.4550	2.8912 ± 1.1853	0.2257 ± 0.1058	15.2769
	1000 samples	29.0807 ± 24.5056	2.9387 ± 1.2339	0.2256 ± 0.1048	7.3601
	2000 samples	28.4729 ± 24.3151	2.9162 ± 1.2021	0.2218 ± 0.1049	3.6720
	5000 samples	28.7922 ± 24.4710	2.9406 ± 1.2192	0.2202 ± 0.1032	1.3554
	10000 samples	28.4612 ± 24.2875	2.8332 ± 1.1765	0.2184 ± 0.1021	0.6216
GMM methods (Ours)	1-sigma region	18.8785 ± 16.4591	1.3750 ± 0.6235	0.1725 ± 0.0783	264.3962
	2-sigma region	18.8595 ± 16.1817	1.3757 ± 0.6182	0.1725 ± 0.0778	271.3125
	3-sigma region	18.8063 ± 15.9940	1.3750 ± 0.6173	0.1725 ± 0.0775	269.7957

TABLE III: Experimental result of the inter-age task.

Methods	Pose error (degree)	Force error (N)	Torque error (Nm)	FPS	
MC methods	50 samples	27.0115 ± 23.2189	2.6255 ± 1.2156	0.1848 ± 0.0874	65.4180
	100 samples	26.4910 ± 22.9918	2.5866 ± 1.1962	0.1843 ± 0.0872	41.4879
	200 samples	26.5139 ± 23.0421	2.5071 ± 1.1539	0.1822 ± 0.0866	33.4342
	500 samples	26.0613 ± 22.8256	2.4649 ± 1.1566	0.1821 ± 0.0852	15.0523
	1000 samples	25.5738 ± 22.7659	2.4177 ± 1.1043	0.1799 ± 0.0845	7.6250
	2000 samples	25.6432 ± 22.7773	2.4564 ± 1.1357	0.1792 ± 0.0838	3.6656
	5000 samples	25.2520 ± 22.6803	2.5137 ± 1.0770	0.1782 ± 0.0829	1.3822
	10000 samples	25.2013 ± 22.4086	2.4153 ± 1.1250	0.1774 ± 0.0830	0.6287
GMM methods (Ours)	1-sigma region	15.5250 ± 14.3686	1.3589 ± 0.8674	0.1032 ± 0.0567	271.0660
	2-sigma region	15.3933 ± 14.3435	1.3587 ± 0.8602	0.1020 ± 0.0557	272.9313
	3-sigma region	15.3966 ± 14.3325	1.3577 ± 0.8577	0.1016 ± 0.0555	275.6897

TABLE IV: Experimental result of the inter-BMI task.

Methods	Pose error (degree)	Force error (N)	Torque error (Nm)	FPS	
MC methods	50 samples	29.8198 ± 22.5163	3.7173 ± 1.6407	0.2190 ± 0.1035	65.8205
	100 samples	29.8195 ± 22.4535	3.7914 ± 1.6415	0.2166 ± 0.1030	43.2587
	200 samples	29.6394 ± 22.6435	3.8630 ± 1.6395	0.2171 ± 0.1013	33.8700
	500 samples	29.2037 ± 22.4719	3.9510 ± 1.6137	0.2172 ± 0.1025	15.1218
	1000 samples	28.9146 ± 22.4461	4.0550 ± 1.6349	0.2131 ± 0.1013	7.4727
	2000 samples	28.8667 ± 22.4426	4.0330 ± 1.6527	0.2129 ± 0.1002	3.6997
	5000 samples	28.6619 ± 22.3158	4.0279 ± 1.6343	0.2100 ± 0.1012	1.4071
	10000 samples	28.1517 ± 22.2918	3.8678 ± 1.6300	0.2071 ± 0.1016	0.6501
GMM methods (Ours)	1-sigma region	22.6850 ± 16.4856	1.6504 ± 0.9148	0.1136 ± 0.0628	285.9330
	2-sigma region	22.6639 ± 16.0608	1.6589 ± 0.9099	0.1145 ± 0.0622	289.1035
	3-sigma region	22.6475 ± 15.6722	1.6620 ± 0.9072	0.1151 ± 0.0624	290.8669